Rapid Communications

Control of Rayleigh-Taylor instability onset time and convective velocity by differential diffusion effects

S. S. Gopalakrishnan,[1,2] J. Carballido-Landeira,[1] B. Knaepen,[2] and A. De Wit[1]
[1]*Nonlinear Physical Chemistry Unit, Université libre de Bruxelles (ULB), CP231, 1050 Brussels, Belgium*
[2]*Service de Physique Statistique et des Plasmas, Université libre de Bruxelles (ULB), CP231, 1050 Brussels, Belgium*

(Received 22 March 2018; published 17 July 2018)

Fingering instabilities of a miscible interface between two fluids in a gravitational field can develop due to adverse density gradients as in the well-known Rayleigh-Taylor (RT) and double-diffusive (DD) instabilities. In the absence of differential diffusion, the mixing rate and the onset time of the RT instability developing when a denser solution of a given solute A overlies a less dense solution of a solute B are respectively proportional and inversely proportional to the initial density difference $\Delta\rho_0$ between the two superposed layers. We show here both experimentally and theoretically for porous media flows that when the mechanisms of RT and DD instabilities are combined, the properties of the convective growth of the fingers are controlled by the dynamic density jump $\Delta\rho_m$ of the nonmonotonic density profile induced by the differential diffusion effects. In particular, the onset time and mixing rate can be controlled by varying the ratio of the diffusion coefficients of the solutes.

DOI: 10.1103/PhysRevE.98.011101

Understanding buoyancy-driven convective processes is of importance due to their ubiquity in various natural and industrial processes ranging from transport of sediments in ground water [1], crystallization in magmas [2], oil recovery [3], carbon sequestration in saline aquifers [4–7], to name a few. Though this field has received a lot of attention in recent years, not much is known about the convective dynamics arising when multiple species contribute to change the density of the fluid.

Specifically, a miscible interface between a denser fluid above a less dense one can deform into buoyancy-driven fingering in a gravitational field because of a Rayleigh-Taylor (RT) instability [8–13]. Previous works on RT fingering have mainly focused on the single specie scenario within a given solvent when a denser solution overlies a less dense solution of the same solute, such that the diffusivity in both solutions is the same. In that case, several experimental and numerical studies of the RT instability for porous media flows have shown that the mean wavelength and the finger length vary in time as $\sqrt{t}$ and t, respectively [8–11,13,14]. The vertical speed at which the fingers ascend or descend is known to scale as the initial dimensional density jump $\Delta\tilde{\rho}_0$ between the two layers while the onset time of the instability decreases when $\Delta\tilde{\rho}_0$ increases [11]. We show here that these scaling laws are changed in the presence of several species diffusing at different rates because of differential diffusion effects.

Convective instabilities also exist in the case of a stratification of less dense fluid above a denser one due to the differential diffusion of components such as salt and heat. Such thermohaline convection has been the subject of numerous studies in particular due to its ubiquity in oceans [15–17]. Laboratory experiments have also focused on the case of two solutes such as salt and sugar which diffuse at different rates [18,19]. In the case of a less dense solution of a solute A overlying a denser solution of solute B, a so-called double-diffusive (DD) instability can deform the miscible interface when $\delta = D_B/D_A > 1$, i.e., when the diffusion coefficient D_B of the lower solute B is sufficiently larger than the diffusion coefficient D_A of the upper solute A. DD fingers (also termed "salt fingers" by analogy with thermohaline convection) develop symmetrically across the initial contact line while the vertical extent of the fingered zone also scales proportionally to t [13]. On the other hand, if $\delta < 1$, a diffusive-layer convection (DLC) instability triggers convective motions above and below the contact line [13].

Recently, the interplay between RT and DLC instabilities has been studied in the case of a denser solution of salt above a less dense solution of sugar, which diffuses roughly three times faster than sugar (i.e., $\delta < 1$). The convective patterns are different from those observed in one specie RT fingering as a Y-shaped "mixed mode" that combines features seen in both RT and DLC instabilities then develops [20]. Scalings of the convective growth have, however, not been addressed.

In this context, we examine here how differential diffusion affects the mixing scales of RT fingering. Specifically, a RT configuration with $\delta > 1$ (such as in the case of DD instability) exhibits a nonmonotonic density profile in which a dimensional density jump $\Delta\tilde{\rho}_m$ develops dynamically because of differential diffusion of the solutes. Depending on the parameters, this density jump $\Delta\tilde{\rho}_m$ can differ significantly from $\Delta\tilde{\rho}_0$, allowing a possible control of the convective mixing zone by using two solutions containing two different solutes diffusing at different rates. Relying on an experimental study of mixing between aqueous solutions of two different solutes in a Hele-Shaw cell, we show that the rate of advancement of the mixing front scales as $\Delta\tilde{\rho}_m$ while the onset time of the instability is inversely proportional to $\Delta\tilde{\rho}_m$. These scaling laws are confirmed and explained by numerical simulations of Darcy's law coupled to evolution equations for the concentrations of the solutes affecting the density of the solution.

In nondimensional form, the convective transport in porous media is described by Darcy's law (1) coupled to evolution

equations for the concentrations of the two species A and B through a constitutive relation for the density ρ [13],

$$\nabla p = -\mathbf{u} + \rho(A,B)\mathbf{y}, \tag{1}$$

$$\nabla \cdot \mathbf{u} = 0, \tag{2}$$

$$A_t + \mathbf{u}\cdot\nabla A = \nabla^2 A, \tag{3}$$

$$B_t + \mathbf{u}\cdot\nabla B = \delta\nabla^2 B, \tag{4}$$

$$\rho(y,t) = A(y,t) + R\,B(y,t), \tag{5}$$

where p is the pressure, $\mathbf{u}$ is the flow velocity, $\mathbf{y}$ is the unit vector in the direction of gravity, A and B are the concentrations of the solutes in the upper and lower solutions, nondimensionalized by their initial concentrations A_0 and B_0, respectively, and ρ is the dimensionless density profile. The two dimensionless parameters of the problem are the ratio of diffusion coefficients δ and the buoyancy ratio $R = (\tilde{\rho}_B - \tilde{\rho}_0)/(\tilde{\rho}_A - \tilde{\rho}_0)$, where $\tilde{\rho}_0$ and $\tilde{\rho}_i$ are the dimensional densities of the solvent and of the solution of $i = A,B$ in initial concentration i_0, respectively.

The initial concentrations in the top layer ($y > 0$) are $A = 1$, $B = 0$, while in the bottom layer ($y < 0$) $A = 0$, $B = 1$. The boundary conditions are $A = 1$, $B = 0$ for $y \to \infty$ and $A = 0$, $B = 1$ for $y \to -\infty$. In the absence of convection, the diffusive base state concentration profiles read

$$A(y,t) = \frac{1}{2}\mathrm{erfc}\left(\frac{y}{2\sqrt{t}}\right), \quad B(y,t) = \frac{1}{2}\mathrm{erfc}\left(-\frac{y}{2\sqrt{\delta t}}\right). \tag{6}$$

Depending on the values of R and δ, these diffusive profiles induce various density profiles (5) and hydrodynamic instabilities [13]. In the absence of differential diffusion ($\delta = 1$), $B = 1 - A$ and the problem can be reduced to a one specie problem for which a RT instability occurs when $R < 1$. If $\delta \neq 1$, a DD instability is obtained for $R > 1$ and $\delta > R^2$ while a DLC instability develops when $R > 1$ and $\delta < 1$.

Our objective here is to investigate the influence of differential diffusion on the onset times and nonlinear convective velocities for the RT instability ($R < 1$) when $\delta > 1$. Initially, the solution of A with dimensional density $\tilde{\rho}_A$ lies above the less dense solution B of density $\tilde{\rho}_B$ and the nondimensional density difference across this step function equals $\Delta\rho_0 = \Delta\tilde{\rho}_0/(\tilde{\rho}_A - \tilde{\rho}_0) = 1 - R$. At later times, the characteristic shape of the purely diffusive density profile [Eq. (5)] then varies significantly depending on the value of δ [Fig. 1(a)]. For $\delta = 1$ (no differential diffusion), the density profile smoothens monotonically in time. However, when $\delta > 1$, the density profile features a nonmonotonic spatial dependence once $t > 0$ [13,20]: As the upward diffusion of solute B is faster than the downward diffusion of solute A, a maximum in density $\rho_{\max}$ appears above the interface and a minimum in density ρ_{min} appears in the lower layer [see Fig. 1(a)]. In other words, differential diffusion induces a dynamic density jump $\Delta\rho_m = \rho_{\max} - \rho_{\min}$. This dynamic density difference $\Delta\rho_m > \Delta\rho_0$ stays constant for $0 < t < \infty$ and is given by

$$\Delta\rho_m = \mathrm{erf}\left(\sqrt{\frac{\ln(\delta/R^2)}{2(1-1/\delta)}}\right) + R\,\mathrm{erf}\left(-\sqrt{\frac{\ln(\delta/R^2)}{2(\delta-1)}}\right). \tag{7}$$

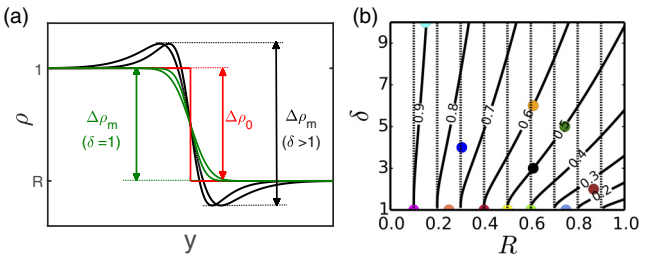

FIG. 1. (a) Temporal evolution of the dimensionless base state density profiles. At $t = 0$, the dimensionless density difference is $\Delta\rho_0$ with $\rho = 1$ for $y < 0$ and $\rho = R$ for $y > 0$ (red line). Later on, the density difference $\Delta\rho_m$ remains equal to $\Delta\rho_0$ only if $\delta = 1$ (green curves) while a nonmonotonic profile with extrema such that $\Delta\rho_m > \Delta\rho_0$ develops if $\delta > 1$ (black curves). (b) Contours of constant $\Delta\rho_m$ (solid lines) and constant $\Delta\rho_0$ (dashed lines) in the (R,δ) plane.

Contours of constant $\Delta\rho_m$ and $\Delta\rho_0$ are plotted in the (R,δ) plane on Fig. 1(b). For small values of R, an increase in δ has little effect on the value of $\Delta\rho_m$, whereas for larger values of R, the effect is pronounced. Also, for a fixed value of δ, increasing R reduces $\Delta\rho_m$. As expected, when $\delta = 1$, $\Delta\rho_m = \Delta\rho_0$, and previous studies on such RT configurations have naturally considered the initial density jump $\Delta\rho_0$ as the scaling for the rate of instability [10,11]. We show below both experimentally and numerically that, when $\delta > 1$, the proper control parameter is $\Delta\rho_m$ and we put forward new scalings for the nonlinear convective regime.

Experiments are conducted in Hele-Shaw (HS) cells which consist of two vertical transparent glass plates separated by a small gap a (ranging between 0.1 and 0.5 mm.) The flow evolution can be described by Darcy's law (1) provided a is small enough with regard to the characteristic length of the dynamics [12,22]. Within the HS cell, the two miscible transparent solutions are put in contact along a horizontal interface by means of a specific injection protocol [23]. The flow dynamics is followed by tracking the gradient of the refractive index of the aqueous solutions using a schlieren technique [24]. Four different solutes for three different gap widths have been considered. The parameters for the related experiments are summarized in the Supplemental Material [21]. The dimensional densities $\tilde{\rho}_0$ (density of pure water), $\tilde{\rho}_A$, and $\tilde{\rho}_B$ have been measured with a DMA 35 Anton Paar density meter. From these values, $\Delta\tilde{\rho}_0 = \tilde{\rho}_A - \tilde{\rho}_B$ and R are computed while δ is obtained for each pair of solutes from Table I of the SM. The nondimensional dynamic density jump $\Delta\rho_m$ is computed theoretically using Eq. (7) and scaled to the dimensional density jump as $\Delta\tilde{\rho}_m = \Delta\rho_m(\tilde{\rho}_A - \tilde{\rho}_0)$.

Figures 2(a) and 2(b) show the RT instability of a denser sucrose solution overlying a less dense KCl solution ($\delta = 3.67$) with identical $\Delta\tilde{\rho}_0 = 0.6\ \mathrm{kg/m^3}$, but different initial concentrations and thus different $\Delta\tilde{\rho}_m$. In both cases, the RT instability is characterized by fingers extending symmetrically across the initial miscible contact line. However, even though $\Delta\tilde{\rho}_0$ is the same, the time to reach the same vertical distance is different. This is confirmed by plotting in Fig. 2(c), for different values of $\Delta\tilde{\rho}_0$, the temporal evolution of the mixing length L defined as the distance between the most upward and downward vertical position of fingers. In all cases, the initial

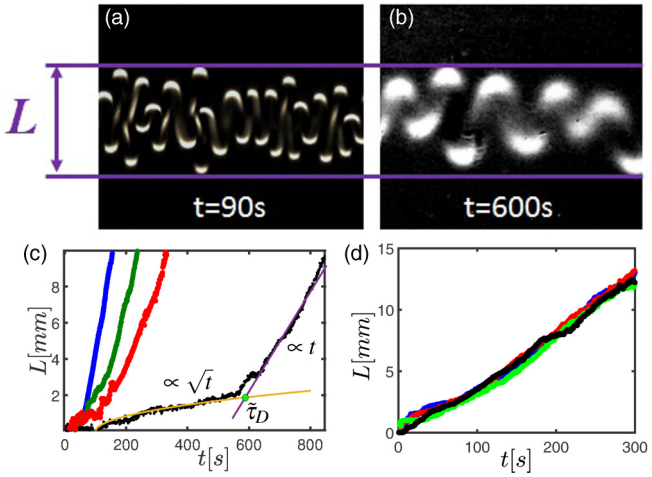

FIG. 2. Experimental snapshots of the RT instability of a denser sucrose solution overlying a less dense KCl solution ($\delta = 3.67$) with equal initial density difference $\Delta\tilde{\rho}_0 = 0.6$ kg/m^3 but $\Delta\tilde{\rho}_m$ equal to (a) 13.8 kg/m^3 (experiment 16) and (b) 1.3 kg/m^3 (experiment 13). Temporal evolution of the mixing length for variable concentrations and (c) $\Delta\tilde{\rho}_0 = 0.6$ kg/m^3 (blue: experiment 16; green: experiment 15; red: experiment 14; black: experiment 13); the onset time, denoted as τ_D, is the time at which the initial diffusive regime is replaced by a regime where a linear increase in time of L is observed; (d) $\Delta\tilde{\rho}_m = 3.7$ kg/m^3 (black: experiment 23; green: experiment 24; blue: experiment 25; red: experiment 26). Parameter values of the experiments are provided in Table II in the Supplemental Material (SM) [21].

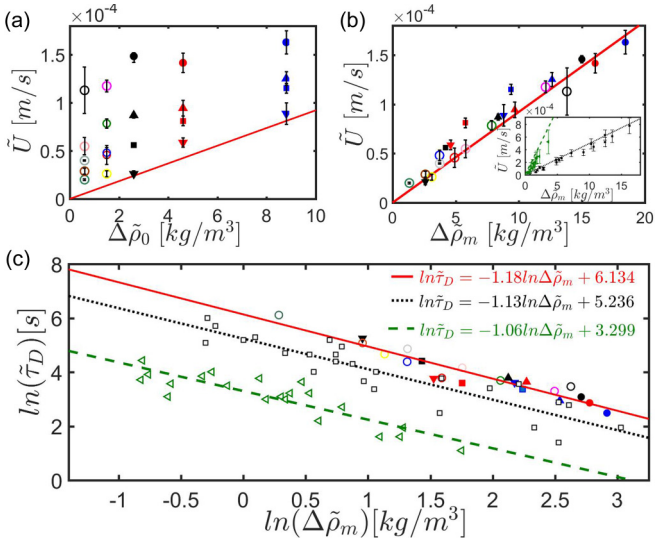

FIG. 3. Experimental mixing velocities in the convective regime for $a = 0.1$ mm as a function of (a) $\Delta\tilde{\rho}_0$ and (b) $\Delta\tilde{\rho}_m$ for $\delta = 1$ (downward triangles), $\delta = 1.25$ (squares), $\delta = 1.89$ (upper triangles), and $\delta = 3.67$ (circles). Solid colors represent experiments with constant $\Delta\tilde{\rho}_0$ but variable $\Delta\tilde{\rho}_m$. Open circles feature different $\Delta\tilde{\rho}_0$ experiments for fixed $\delta = 3.67$. The continuous lines in (a) and (b) are the equations $\tilde{U} = gK\Delta\tilde{\rho}_0/\mu$ and $\tilde{U} = gK\Delta\tilde{\rho}_m/\mu$, respectively. The inset in (b) shows the mixing velocity for two other gap widths: 0.25 mm (solid line) and 0.5 mm (dotted line). See Supplemental Material [21] for details on parameter values. (c) Dependence of the onset time $\tilde{\tau}_D$ on $\Delta\tilde{\rho}_m$ for variable gap widths $a = 0.1$ mm (solid line), $a = 0.25$ mm (dotted line), and $a = 0.5$ mm (dashed line).

diffusive regime during which L grows as $\sqrt{t}$ is followed by a linear increase in time of L. The time at which the deviation between both regimes is observed is denoted as the onset time τ_D and is computed as shown in Fig. 2(c). Even though $\Delta\tilde{\rho}_0$ is kept constant in Fig. 2(c), we observe that both τ_D and the growth rate of the fingers in the linear regime are different in all cases. Quite strikingly, if we now plot in Fig. 2(d) the temporal evolution of L for different experiments characterized by the same value of $\Delta\tilde{\rho}_m$, we observe that the growth rate and the onset times are identical in all cases. This indicates that the proper scaling for the rate of instability in the configuration considered is not the initial density jump $\Delta\tilde{\rho}_0$, but rather the dynamic density jump $\Delta\tilde{\rho}_m$.

To further support those observations, dimensional mixing velocities $\tilde{U}$ (defined as the average of $\Delta L/\Delta t$ in the nonlinear regime) and onset times $\tilde{\tau}_D$ have been measured for three different gap widths a and various pairs (R,δ) values by varying the nature of the solutes and their concentrations (see Supplemental Material [21]). As an example, for $a = 0.1$ mm, we have analyzed the convective dynamics of a denser solution of either sucrose, glycerol, NaCl, or KCl over a less dense solution of KCl (giving $\delta = 3.67$, 1.89, 1.25, and 1, respectively) for different initial concentrations and thus variable R, $\Delta\tilde{\rho}_0$, and $\Delta\tilde{\rho}_m$. Figure 3(a) shows that, at fixed $\Delta\tilde{\rho}_0$, the mixing velocity increases when varying δ and thus $\Delta\tilde{\rho}_m$ (resulting in vertical velocities $\tilde{U}$ up to five times larger for $\delta = 3.67$ than for $\delta = 1$). Only the experiments with $\delta = 1$ (downwards triangles) follow the trend $\tilde{U} = gK\Delta\tilde{\rho}_0/\mu$ (solid red line) where the permeability $K = a^2/12$. In contrast, a linear trend $\tilde{U} = gK\Delta\tilde{\rho}_m/\mu$ is observed when all velocities $\tilde{U}$ are plotted as a function of the dynamic density jump $\Delta\tilde{\rho}_m$ [Fig. 3(b)]. A similar scaling is obtained for experiments with two other gap widths ($a = 0.25$ mm and $a = 0.5$ mm) as shown in the inset in Fig. 3(b) with an increase in the slope when the permeability K increases with the gap width. Note that some deviations from the theoretical trend $\tilde{U} = gK\Delta\tilde{\rho}_m/\mu$ are observed for the largest gap width $a = 0.5$ mm. This is expected as when the gap width of the Hele-Shaw cell is increased, Darcy's law no longer holds [11]. Similarly, we find experimentally that the onset time $\tilde{\tau}_D$ scales inversely to $\Delta\tilde{\rho}_m$ for all three gap thicknesses analyzed over a large range of (R,δ) values [see Fig. 3(c)]. A regression analysis gives $\ln(\tilde{\tau}_D) = C\ln(\Delta\tilde{\rho}_m) + D$ with C varying from -1.18 to -1.06 depending on the gap width and D a constant decreasing with a.

To verify the experimental scalings and understand why the onset time of convection and the velocity of advancement of the fingering zone scale as a function of $\Delta\tilde{\rho}_m$ rather than $\Delta\tilde{\rho}_0$, we turn to numerical simulations of the nondimensional Eqs. (1)–(5) using the finite-volume code YALES2 [25]. The numerical simulations were carried out in a box large enough for the dynamics not to be influenced by the upper and lower boundaries with around 100 fingers developing below the interface. The instability was triggered by adding a small amount of noise with an amplitude of 0.1% on the initial concentration field throughout the entire domain. An example of the density field in the RT instability is shown in Fig. 4(c). In Fig. 4(a), we plot the dimensionless mixing velocity U as

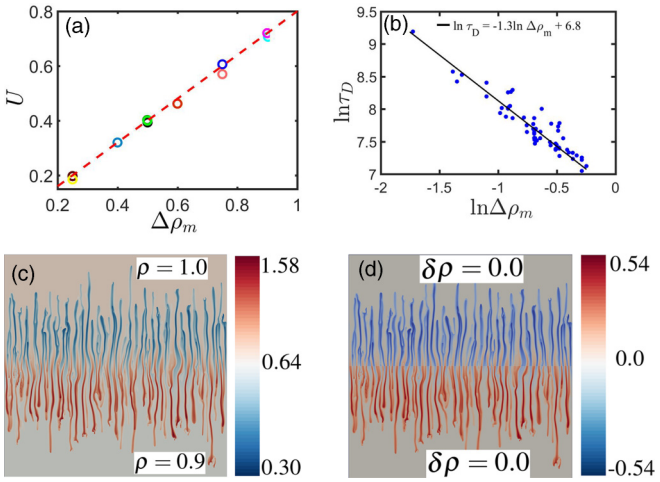

FIG. 4. (a) Mixing velocity U computed as the average value of $\Delta L/\Delta t$ (see Fig. 1 given in the Supplemental Material [21]) in the convective regime as a function of $\Delta\rho_m$. The color code used for the dotted symbols is the same as in the Supplemental Material [21]. The dotted red line shows the linear fit $U = 0.8\Delta\rho_m$. (b) Onset time τ_D as a function of $\Delta\rho_m$. Spatial distribution of (c) the density field ρ and (d) the difference $\delta\rho$ with the initial density for $R = 0.90$, $\delta = 10.0$, $\Delta\rho_0 = 0.10$, $\Delta\rho_m = 0.54$.

a function of the dimensionless $\Delta\rho_m$ for the different (R,δ) values considered (see Supplemental Material [21]). Cases having the same value of $\Delta\rho_m$ have the same mixing velocity and, as in the experiments, we observe a linear relationship between U and $\Delta\rho_m$, i.e., $U = 0.8\Delta\rho_m$. We note that the proportionality coefficient is, however, slightly different. This could originate from the difference in initial conditions between the experiments and the numerical simulations, a feature also observed when studying the scalings of the RT instability in hydrodynamic flows [26]. In Fig. 4(b), we plot the onset time τ_D (defined as in the experiments) as a function of $\Delta\rho_m$ and we again observe that it is inversely proportional to the dynamic density jump.

The relevance of $\Delta\rho_m$ in the control of the growth of convection can be understood by analyzing the density field at a given time in the nonlinear regime as shown in Figs. 4(c) and 4(d). In this example, $\rho_A = 1.0$, $\rho_B = 0.9$, $\delta = 10$, $R = 0.9$ giving, respectively, $\Delta\rho_0 = 0.1$ and $\Delta\rho_m = 0.54$. The difference in density $\Delta\rho_0$ between the two bulk solutions is here relatively small, but the color code of Fig. 4(c) shows that the density in the sinking (rising) fingers can reach much larger (smaller) values than ρ_A (ρ_B) because of the extrema in density dynamically induced by differential effects. The role on the convective dynamics of these extrema in density can be better seen in Fig. 4(d), showing the quantity $\delta\rho = \rho(y,z,t) - \rho(y,z,0)$. Far away from the convective zone, we obviously have $\delta\rho = 0$. However, the density difference between the fingers and their surroundings is such that $\delta\rho \sim \pm 0.54$ and that, quite strikingly, this value is equal to $\Delta\rho_m$. This shows that, even though the initial density jump is $\Delta\rho_0$, differential diffusion induces right from the beginning a nonmonotonic density profile such that fingers experience a density jump $\Delta\rho_m$ with the bulk solution surrounding them. As a consequence, the fingers' convective velocity remains constant and is fixed by $\Delta\rho_m$.

In summary, we have shown both experimentally and numerically that the dynamic density jump that develops in time after contact between two miscible solutions containing two solutes diffusing at different rates governs the properties of the RT instability. In particular, the finger velocity scales linearly while the onset time varies inversely to this density difference, which is a function of the ratio R of initial densities and ratio δ between the diffusion coefficients of the solutes involved. These new scalings allow for control of RT convective mixing by double-diffusive effects. As these differential diffusion features control the density profile independently of the flow equation, it is expected that similar effects will be obtained with Navier-Stokes flows as well, which paves the way to revisiting in depth the RT instability properties in multispecies solutions.

We acknowledge the ARC CONVINCE programme for financial support and computational resources on the Tier-1 supercomputer of the Fédération Wallonie-Bruxelles funded by the Walloon Region under Grant Agreement No. 1117545. J.C.-L. has benefited from a FRS-FNRS fellowship.

S.S.G. and J.C.-L. contributed equally to this work.

[1] T. Green, Scales for double-diffusive fingering in porous media, Water Resour. Res. **20**, 1225 (1984).

[2] H. E. Huppert and R. S. J. Sparks, Double-diffusive convection due to crystallization in magmas, Annu. Rev. Fluid Mech. **12**, 11 (1984).

[3] T. Menand and A. W. Woods, Dispersion, scale, and time dependence of mixing zones under gravitationally stable and unstable displacements in porous media, Water Resour. Res. **41**, W05014 (2005).

[4] S. Backhaus, K. Turitsyn, and R. E. Ecke, Convective Instability and Mass Transport of Diffusion Layers in a Hele-Shaw Geometry, Phys. Rev. Lett. **106**, 104501 (2011).

[5] A. C. Slim, Solutal-convection regimes in a two-dimensional porous medium, J. Fluid Mech. **741**, 461 (2014).

[6] V. Loodts, C. Thomas, L. Rongy, and A. De Wit, Control of Convective Dissolution by Chemical Reactions: General Classification and Application to CO_2 Dissolution in Reactive Aqueous Solutions, Phys. Rev. Lett. **113**, 114501 (2014).

[7] J. J. Hidalgo, J. Fe, L. Cueto-Felgueroso, and R. Juanes, Scaling of Convective Mixing in Porous Media, Phys. Rev. Lett. **109**, 264503 (2012).

[8] R. A. Wooding, Growth of fingers at an unstable diffusing interface in a porous medium or Hele-Shaw cell, J. Fluid Mech. **39**, 477 (1969).

[9] O. Manickam and G. M. Homsy, Fingering instabilities in vertical miscible displacement flows in porous media, J. Fluid Mech. **288**, 75 (1995).

[10] J. Fernandez, P. Kurowski, L. Limat, and P. Petitjeans, Wavelength selection of fingering instability inside Hele-Shaw cells, Phys. Fluids **13**, 3120 (2001).

[11] J. Fernandez, P. Kurowski, P. Petitjeans, and E. Meiburg, Density-driven unstable flows of miscible fluids in a Hele-Shaw cell, J. Fluid Mech. **451**, 239 (2002).

[12] J. Martin, N. Rakotomala, and D. Salin, Gravitational instability of miscible fluids in a Hele-Shaw cell, Phys. Fluids **14**, 902 (2002).

[13] P. M. J. Trevelyan, C. Almarcha, and A. De Wit, Buoyancy-driven instabilities of miscible two-layer stratifications in porous media and Hele-Shaw cells, J. Fluid Mech. **670**, 38 (2011).

[14] S. S. Gopalakrishnan, J. Carballido-Landeira, A. De Wit, and B. Knaepen, Relative role of convective and diffusive mixing in the miscible Rayleigh-Taylor instability in porous media, Phys. Rev. Fluids **2**, 012501 (2017).

[15] J. S. Turner, *Buoyancy Effects in Fluids* (Cambridge University Press, Cmabridge, U.K., 1979).

[16] T. Radko, *Double Diffusive Convection* (Cambridge University Press, Cmabridge, U.K., 2013).

[17] R. W. Schmitt, Double diffusion in oceanography, Annu. Rev. Fluid Mech. **26**, 255 (1994).

[18] S. E. Pringle and R. J. Glass, Double-diffusive finger convection: influence of concentration at fixed buoyancy ratio, J. Fluid Mech. **462**, 161 (2002).

[19] C. A. Cooper, R. J. Glass, and S. W. Tyler, Experimental investigation of the stability boundary for double-diffusive finger convection in a Hele-Shaw cell, Water Resour. Res. **33**, 517 (1997).

[20] J. Carballido-Landeira, P. M. J. Trevelyan, C. Almarcha, and A. De Wit, Mixed-mode instability of a miscible interface due to coupling between Rayleigh-Taylor and double-diffusive convective modes, Phys. Fluids **25**, 024107 (2013).

[21] See Supplemental Material at http://link.aps.org/supplemental/10.1103/PhysRevE.98.011101 for the parameter values of the experiments.

[22] E. Guyon, J.-P. Hulin, L. Petit, and C. Mitescu, *Physical Hydrodynamics* (Oxford University Press, Oxford, U.K., 2001).

[23] Y. Shi and K. Eckert, A novel Hele-Shaw cell design for the analysis of hydrodynamic instabilities in liquid-liquid systems, Chem. Eng. Sci. **63**, 3560 (2008).

[24] G. S. Settles, *Schlieren and Shadowgraph Techniques* (Springer, Berlin, 2001).

[25] V. Moureau, P. Domingo, and L. Vervisch, Design of a massively parallel CFD code for complex geometries, C. R. Mec. **339**, 141 (2011).

[26] J. D. Youngs, Rayleigh-Taylor mixing: Direct numerical simulation and implicit large eddy simulation, Phys. Scr. **92**, 074006 (2017).